# Effects of shear direction on the shearing behavior of a soil-structural interface using discrete element method

Wei-Bin Chen, Wan-Huan Zhou, Xue-Ying Jing
*Faculty of Science and Technology, University of Macau, Macau, China and UMacau Research Institute, Zhuhai, Guangdong, China, hannahzhou@umac.mo*

ABSTRACT: To investigate the effects of shear direction on the shear behavior of a soil-structural interface and the shear banding in it, a series of three-dimensional numerical interface shear tests considering various angles of shear direction, defined as the angle between the shear direction and the direction of a surface's roughness anisotropy, are performed using the discrete element method. Simulation results show that (1) shear stress increases with an increasing of the angle of shear direction, with the elastic perfect-plasticity observed when the angle of shear direction equals zero; (2) all specimens show bulk dilatancy during the shearing process, increasing with the angle of shear direction; and (3) peak stress increases with the angle of shear direction, as does the thickness of the shear band.

RÉSUMÉ: Pour étudier l'effet de la direction de cisaillement sur le comportement mécanique en cisaillement de l'interface sol-structure et de la bande de cisaillement, une série d'essais numérique en trois-dimensions de cisaillement d'interface en considération différents angles de direction de cisaillement, définie comme l'angle inclus entre la direction de cisaillement et la direction d'une anisotropie de rugosité de surface. Les résultats montrent que: (1) la contrainte de cisaillement augmente avec une augmentation de l'angle de direction de cisaillement, et la plasticité élastique parfaite est observée lorsque l'angle de direction de cisaillement est égal à zéro, (2) tous les spécimens montrent une volume dilatance pendant le processus de cisaillement, la dilatance augmente avec l'angle de direction de cisaillement; et (3) la contrainte de crête augmente avec l'angle de direction de cisaillement comme l'épaisseur de la bande de cisaillement.

KEYWORDS: soil-structure interface, discrete element method, shear direction, shear behavior.

## 1 INTRODUCTION

The interaction between soil and structure is an important topic in geotechnical engineering, being integral to things such as soil–pile interaction, soil–retaining wall contact, and soil–foundation contact. Various studies have shown that the shear behavior of a soil-structure interface is related to the physical characteristics of soil, as well as to the structure's surface roughness, the condition of experiment loading and so forth (Jensen et al. 1999, Frost et al. 1999, Zeghal and Edil 2002, Hu and Pu 2004, Zhang et al. 2006, Wang et al. 2007, Yin and Zhou 2009, DeJong and Westgate 2009, Taha and Fall 2012). Among a variety of influencing factors, the decisive effect of rough surface geometry on soil's performance under interface shearing has been stressed time and again in the literature (Hu and Pu 2004, Wang et al. 2007, Filz et al. 2008, Chen et al. 2015). In engineering practice, a structural surface's geometry likely possesses a certain degree of intrinsic anisotropy as a result of the nature of the material that makes up the structure as well as of the engineering skills and craftsmanship that contributed to its creation. This uneven asperity spatially distributes on the surface—not isotropically but rather tending in certain directions. Accordingly, shear behavior differs when soil is sheared from different directions. Yet few studies have contributed to the body of knowledge surrounding this phenomenon, leaving us little recourse for discovering how much, and in what way, the mechanical performance of a soil–structural interface depends on shear direction.

This study investigates the effects of shear direction on the shear behavior of a soil–structural interface and shear banding in it, particularly by analyzing the mechanical performance and kinematics of granular soil. Using the discrete element code PFC3D, a series of three-dimensional numerical interface shear tests were performed, that considered various shear directions. This paper first introduces the modeling approach used and the laboratory validation of numerical results, then discusses the effects of shear direction on the shear behavior of a soil–structural interface and the shear banding in it.

## 2 DEM MODEL AND PARAMETERS

The simulated interface direct shear device is an 80 mm (length) × 80 mm (width)× 34 mm (height) shear box enclosed by four rigid lateral walls, a top boundary for applying normal stress, and a rough bottom plate with saw-teeth sloped 45°, as schematically shown in Figures 1, 2, and 3. The rough plate shears at the same profile, when viewed along *y*-axis, and the preferential direction in the model is defined to be aligned heading the x-axis. This study considers five angles of shear direction θ (0°, 30°, 45°, 60°, 90°), defined as the angle of shear direction and the direction of surface's roughness anisotropy (along the *y*-axis), with the bottom plate unchanged ($R_n$ = 1). The relative roughness $R_n$ is defined by $R_n = R_{max}/D_{50}$, where $R_{max}$ is the vertical distance between the highest peak and the lowest valley along a profile length) over $D_{50}$ (mean grain size). Figure 2 shows the case when the angle of shear direction equals 90°.

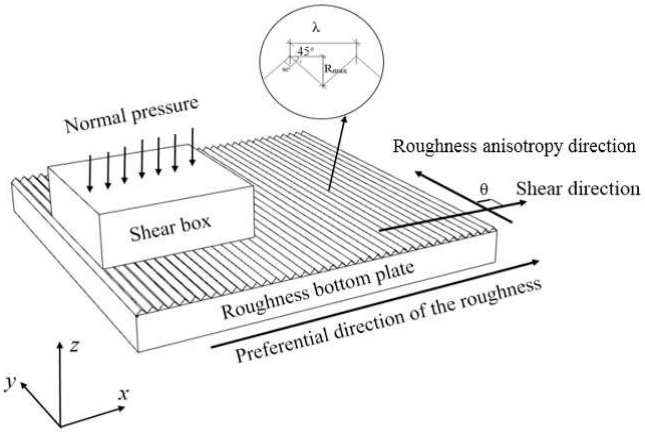


Figure 1. Schematic diagram of the numerical interface shear test

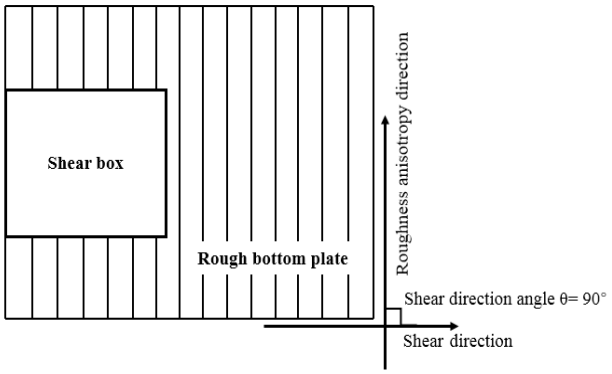


Figure 2. Overhead view of the numerical interface shear test (θ = 90°)

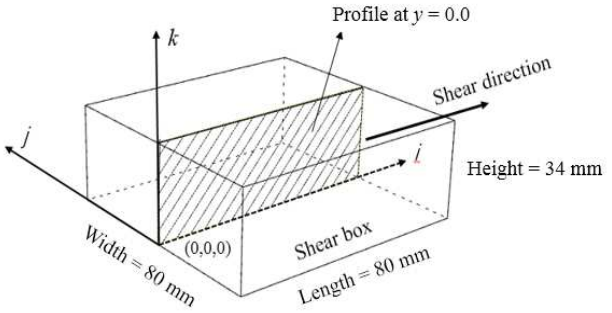


Figure 3. Schematic diagram of the shear box in the local coordinate of the shear box

Particles were generated within the shear box using a grain size distribution corresponding to Fujian sand (used later to validate the numerical model), having a medium particle size ($D_{50}$) of 2.55$mm$, as shown in Figure 4. (The particle size used in numerical simulations is 2 times greater than that found in real Fujian sand.) Next, the confining pressure was applied to the top boundary as well as to fours lateral boundaries until the desired pressure was reached using a servo control mechanism. This study considered four levels of confinement for each specimen: 50, 150, 200 and 300 kPa. Finally, a constant horizontal velocity of 0.1 *mm/min* was exerted on the bottom plate, while keeping the four lateral boundaries fixed and keeping the normal pressure $\sigma_n$ being equal to the value at the confining section.

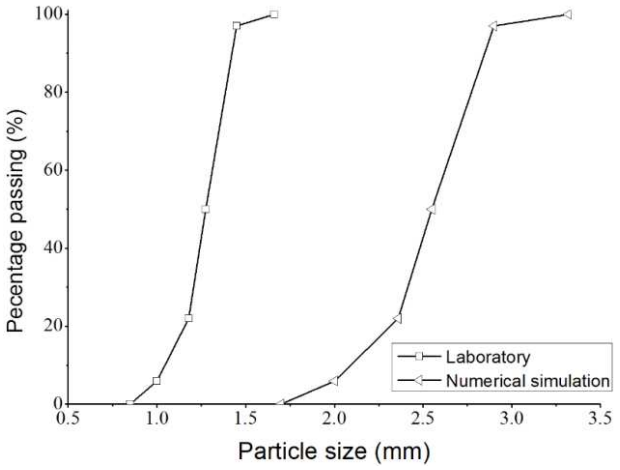


Figure 4. Particle size distributions in laboratory testing and in numerical simulation

Table 1. Relevant parameters in interface shear tests

| Parameters | Value |
|---|---|
| Ball density (kg/m$^3$) | 2650 |
| Initial porosity | 0.32 |
| Inter-particle normal stiffness (N/m) | $0.7\times10^7$ |
| Inter-particle shear stiffness (N/m) | $0.35\times10^7$ |
| Particle-wall normal stiffness (N/m) | $1.0\times10^8$ |
| Particle-wall shear stiffness (N/m) | $0.5\times10^8$ |
| Inter-particle friction coefficient | 0.3 |
| Particle-wall friction coefficient | 0.2 |
| Inter-particle rolling resistance coefficient | 0.05 |

The linear contact model with friction was used to define interactions between contacting objects, with the friction angle 17.0° for particle–particle contacts and 11.0° for particle–wall contacts. Moreover, application of a particle rolling resistance model to the contacts helped mimic the shape effect of grains on shear behavior in soil–structural interaction. The particle–bottom boundary friction coefficient used in this study, $\tan\varphi_\mu$—that is, 0.05—embodies the friction coefficient of a single particle sliding against solid surfaces. Each simulation featured about 65,000 spherical particles. Table 1 summarizes other modeling parameters relevant to these analyses.

Three laboratory interface shear tests (angle of shear direction θ = 90°; $\sigma_n$ = 50, 100, 200 kPa) using Fujian sand, having the grain size distribution plotted in Figure 4 helped validate the numerical simulation. Figure 5 shows the evolution of shear stress in terms of the shear displacement obtained in laboratory tests and in numerical simulations (under the same shearing conditions as in the laboratory tests). As can be seen, the curves obtained exhibit similar peak shear stresses and, arguably, similar final stresses even though the curve produced by the numerical simulation shows greater fluctuation after reaching a peak state. Overall, the results obtained through numerical simulation agree well with laboratory results.

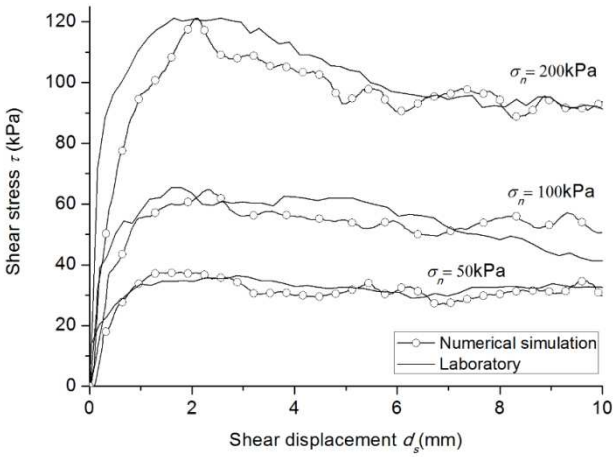


Figure 5. Shear stress versus shear displacement in laboratory testings and in numerical simulations

## 3 RESULTS AND DISCUSSION

This section, by analyzing the mechanical performance and kinematics of the specimens, traces the effects of shear direction on the shear behavior of a soil–structural interface and shear band thickness.

### 3.1 *Shear behavior*

Figures 6 and 7 show the shear stress ratio $\tau/\sigma_n$ and volumetric strain $\varepsilon_v$ against shear displacement, where $\tau$ is the shear stress exerted on the rough bottom plate; $\varepsilon_v = \Delta l/l$, $\Delta l$ is the change of normal deformation; and $l$ is the initial sample height. Figure 7 shows that shear stress levels increase with the angle of shear direction. A failure model of elastic perfect–plasticity seemingly exists when θ=0°, with an

extremely straight line of $\tau/\sigma_n$ observed after reaching the peak stress ratio. when θ = 90°, by contrast, the curve shows obvious fluctuations after reaching the peak stress ratio. The shear behavior of the interface demonstrates strain softening when θ = 30°, 45°, 60°, 90°. Moreover, Figure 6 indicates that the shear behavior of the interface when θ=30°, 45°, 60°, and 90° shows bulk dilatancy during the shearing process, increasing with the angle of shear direction. Interestingly, a slight degree of bulk dilatancy is evident when θ= 0°.

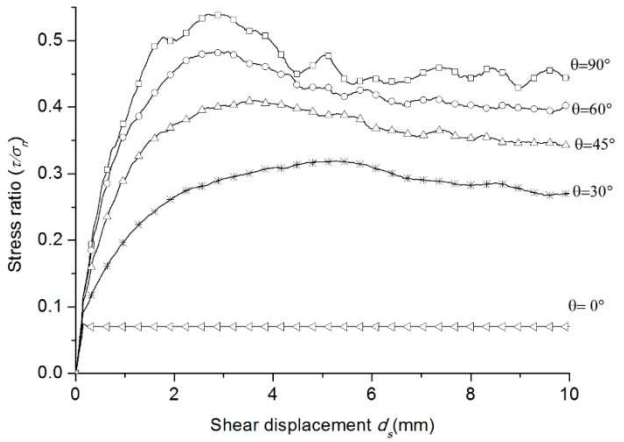


Figure 6. Stress ratio (τ/σₙ) with respect to shear displacement for various angles of shear direction (σₙ = 300 kPa)

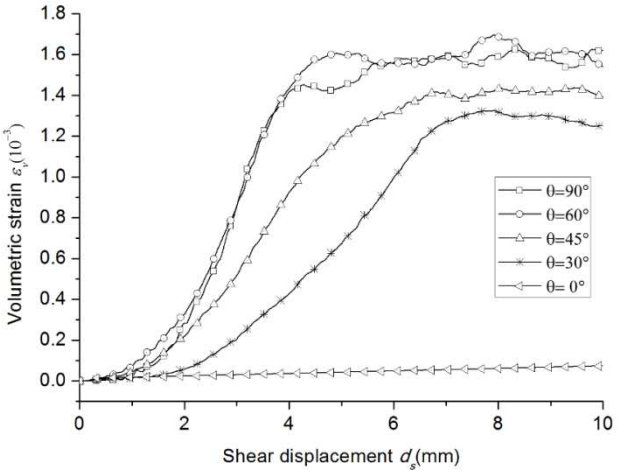


Figure 7. Volumetric strain with respect to shear displacement for various angles of shear direction (σₙ = 300 kPa)

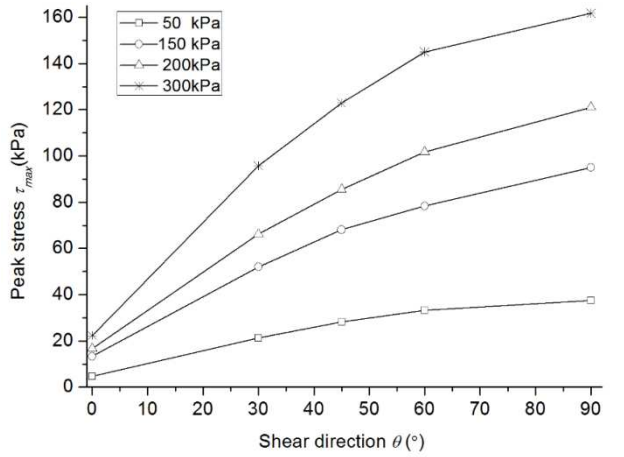


Figure 8. Peak stress against angles of shear direction for various normal degree of stress

Figure 8 shows variations in the maximum shear stress $\tau_{max}$ with the angle of shear direction. The peak shear stress $\tau_{max}$ increases with the angle of shear direction under confining pressures of 50, 150, 200, 300 kPa. Accordingly, specimens having a shear direction nearer to the perpendicular direction can achieve greater levels of shear stress, with maximum shear strength achieve when the shear direction is perfectly perpendicular to surface's direction of roughness anisotropy (θ = 90°)—that is, the direction of maximal interface resistance to the soil.

### 3.2 *Shear band thickness*

When the angle of shear direction changes, it likely influences the specimen's kinematical development. Figures 8(a), (b), and (c) show the $x$-direction velocity distribution field at a cross-section ($y$ = 0.0, shown in Figure 3) of the specimen having a shear displacement of $d_s = 2.5mm$ (σₙ = 300 kPa) and with the angle of shear direction angles at 90°, 45° and 0°, respectively. Notably, the shear bands produced by high angles of shear direction are thicker than those produced by low angles of shear direction. Indeed, when θ = 0°, no shear band is evident.

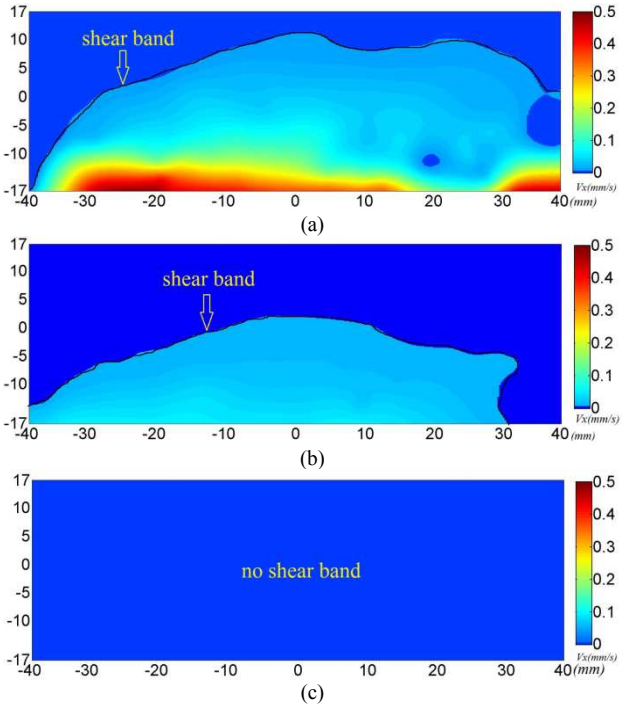


Figure 9. $x$-direction velocity distribution field of particles at $d_s = 2.5mm$ (σₙ = 300 kPa): (a) at θ = 90°; (a) at θ = 45°; (c) at θ = 0°

### 3.3 *Discussion*

The shear resistance of a rough surface is significantly influenced by the shear direction when the rough surface has a natural anisotropy. When θ = 90°, and the shear direction is orthogonal to the direction of a surface's roughness anisotropy, the rough surface's resistance to the soil has been completely mobilized, in turn maximizing the corresponding shear strength, as shown in Figure 8. Moreover, the thickness of the shear band is greatest when θ = 90°, with the resulting values 8~10 times the mean particle diameter ($D_{50} = 2.55mm$), as shown in Figure 9(a).

when θ = 0°, with the shear direction parallel to the direction of a surface's roughness anisotropy, shear strength reaches its lowest value, and the shear failure occurs only at the interface between the soil and the rough surface. Thus shear strength depends, in this instance, entirely on particle–surface friction. This is the reason why a failure model of elastic perfect-

plasticity can be observed in Figure 6 and no shear band is evident in Figure 9(c).

when $\theta = 30°$, 45°, or 60°, the soil's shear resistance can be decomposed into two components. The one vertical to shear direction is the main resource of the soil's shear resistance, while the another component parallel to the shear direction can be considered secondarily in terms of giving rise the soil's shear resistance. Accordingly, the stress ratio decreases with the angle of shear direction, as shown in Figure 6.

## 4 CONCLUSION

A series of three-dimensional numerical interface shear tests were performed using the discrete element code PFC3D by considering various angles of shear direction. Some conclusions can be draw: (1) shear stress increases with an increasing of the angle of shear direction, with the elastic perfect-plasticity observed when the angle of shear direction equals zero; (2) all specimens show bulk dilatancy during the shearing process, increasing with the angle of shear direction; and (3) peak stress increases with the angle of shear direction, as does the thickness of the shear band. Indeed, when $\theta = 0°$, no shear band is evident.

## 5 ACKNOWLEDGEMENTS

The authors gratefully acknowledge the financial support from the National Natural Science Foundation of China (Grant no. 51508585), the Macau Science and Technology Development Fund (FDCT/125/2014/A3) and the University of Macau Research Fund (Grant nos. MYRG2014-00175-FST and MYRG2015-00112-FST).

## 6 REFERENCES

Chen X.B. et al. 2015. Effect of roughness on shear behavior of red clay–concrete interface in large-scale direct shear tests. *Canadian Geotechnical Journal* 52 (8), 1122-1135.

DeJong J.T. and Westgate Z.J. 2009. Role of initial state, material properties, and confinement condition on local and global soil-structure interface behavior. *Journal of geotechnical and geoenvironmental engineering*135 (11), 1646-1660.

Filz G.M., Gómez J.E., Dove J.E., and Ebeling R.M. 2008. Sand-to-concrete interface response to complex load paths in a large displacement shear box. *Geotechnical Testing Journal* 31 (4), 1-12.

Frost J.D. and Han J. 1999. Behavior of interfaces between fiber-reinforced polymers and sands. *Journal of geotechnical and geoenvironmental engineering* 125 (8), 633-640.

Hu L.M. and Pu J.L. 2004. Testing and Modeling of Soil-Structure Interface. *Journal of geotechnical and geoenvironmental engineering* 130 (8), 851-860.

Itasca Consulting Group Inc. 2015. PFC3D User's manual, version 5.0. Minnesota: Itasca Consulting Group.

Jensen R.P., Bosscher P.J., Plesha M.E., and Edil T.B. 1999. DEM simulation of granular media—structure interface: effects of surface roughness and particle shape. *International Journal for Numerical and Analytical Methods in Geomechanics* 23 (6), 531-547.

Taha A. and Fall M. 2012. Shear behavior of sensitive marine clay-concrete interfaces. *Journal of geotechnical and geoenvironmental engineering* 139 (4), 644-650.

Uesugi M. and Kishida H. 1986. Frictional resistance at yield between dry sand and mild steel. *Soils Found* 26 (4), 139-149.

Wang J.F., Joseph E.D. and Gutierrez M.S. 2007. Anisotropy-Based Failure Criterion for Interphase Systems. *Journal of geotechnical and geoenvironmental engineering* 133 (5), 599-608.

Yin, J. H. and Zhou, W. H. 2009. Influence of grouting pressure and overburden stress on the interface resistance of a soil nail. *Journal of Geotechnical and Geoenvironmental Engineering* 135 (9), 1198-1208.

Zeghal M. and Edil T.B. 2002. Soil structure interaction analysis: modeling the interface. *Canadian Geotechnical Journal* 39 (3), 620-628.

Zhang G. and Zhang J.M. 2006. Monotonic and cyclic tests of interface between structure and gravelly soil. *Soils and foundations* 46 (4), 505-518.